

## Article

# Multi-Objective Lightweight Optimization Design of the Aluminium Alloy Front Subframe of a Vehicle

Xiangchao Meng<sup>1,2</sup>, Youping Sun<sup>1,2,3,\*</sup>, Jiangmei He<sup>3</sup>, Wangzhen Li<sup>1,2</sup> and Zhifeng Zhou<sup>4</sup>

<sup>1</sup> School of Mechanical and Transportation Engineering, Guangxi University of Science and Technology, Liuzhou 545006, China

<sup>2</sup> Guangxi Earthmoving Machinery Collaborative Innovation Center, Liuzhou 545006, China

<sup>3</sup> Guangxi Key Laboratory of Automobile Components and Vehicle Technology, Guangxi University of Science and Technology, Liuzhou 545006, China

<sup>4</sup> Liuzhou Wuling New Energy Automobile Co., Ltd., Liuzhou 545007, China

\* Correspondence: syptajji@126.com

**Abstract:** The aluminium alloy front subframe of an automobile was developed through multi-operating condition topology optimization and multi-objective optimization methods. By considering the influences of loads on the strength, static stiffness, and modal of the aluminium alloy front subframe under typical operating conditions, the performance parameters of the aluminium alloy front subframe after topology optimization were obtained. After topology optimization was performed, the parametric model of the aluminium alloy front subframe was established. Based on the Isight optimization platform, sample points were generated with the optimal Latin hypercube test method, and the response surface approximate model was constructed. The minimum mass and maximum first-order frequency were taken as the objectives, the stress under typical working conditions did not exceed the set target value, and the maximum displacement of the installation point was taken as the constraint condition. The multi-objective particle swarm optimization algorithm was used to optimize the aluminium alloy front subframe. The error of the free modal and finite element free modal analysis of the aluminium alloy front subframe samples was less than 15%. The optimized aluminium alloy front subframe was 2.4 kg lighter than the original subframe under the premise of satisfying various performance indices, and the lightweight rate was up to 12%.

**Keywords:** multi-condition topology optimization; aluminium alloy front subframe; Isight; optimal Latin hypercube; response surface approximate model; multi-objective particle swarm optimization algorithm



**Citation:** Meng, X.; Sun, Y.; He, J.; Li, W.; Zhou, Z. Multi-Objective Lightweight Optimization Design of the Aluminium Alloy Front Subframe of a Vehicle. *Metals* **2023**, *13*, 705. <https://doi.org/10.3390/met13040705>

Academic Editor: Badis Haddag

Received: 3 March 2023

Revised: 28 March 2023

Accepted: 30 March 2023

Published: 4 April 2023



**Copyright:** © 2023 by the authors. Licensee MDPI, Basel, Switzerland. This article is an open access article distributed under the terms and conditions of the Creative Commons Attribution (CC BY) license (<https://creativecommons.org/licenses/by/4.0/>).

## 1. Introduction

The subframe is an auxiliary device connecting the suspension connector and the body. It is an important part of the chassis. The traditional subframe is made of steel, which undoubtedly increases the weight of the whole vehicle. Studies have shown that for every 100 kg reduction in the vehicle weight, fuel consumption will be reduced by approximately 0.4 L per 100 km, and CO<sub>2</sub> emissions will be reduced by 8 to 11 g [1]. With the rise of new energy vehicles, an increasing number of automobile enterprises have begun to use aluminium alloy subframes. Using aluminium alloy subframes not only improves vehicle handling and stability but also reduces the weight of the vehicle. The production mode of aluminium alloy subframes mainly includes the extruded profile welding type and casting type. In recent years, many scholars have performed research on the development of subframes and have obtained some research results. Li et al. [1] proposed a subframe topology optimization method from a conceptual design to a detailed design, which further reduced the overall subframe weight, met the requirements of stiffness and natural frequency, passed the durability requirements, and, finally, reduced the subframe mass from the initial structure of 82.6 kg to 21.4 kg. Kim et al. [2] proposed a subframe method based on

topology optimization, which took the bar section and stiffness value as the design variables to simultaneously optimize the topology and shape of the subframe. Ali and Fraser [3] used the finite element method to analyse a certain subframe of a Chevrolet vehicle, used LS-DYNA commercial software to model the subframe, analysed the subframe under normal driving conditions and vehicle collision conditions, and established the appropriate subframe material by comparison with the performance of the original subframe of the vehicle. Nam et al. [4] proposed a fatigue life evaluation technology for the aluminium subframes of automobiles. Based on the virtual test simulation technology of the nonlinear suspension component model, this technology can effectively predict the fatigue life of the vehicle chassis structure. By testing an actual aluminium subframe, the accuracy of the model was verified. Lee et al. [5] optimized the shape and thickness of the subframe to meet the requirements of multidisciplinary design optimizations (MDOs) and meet the weight, fatigue, crash, NVH, and K & C performance requirements. The proposed method was also suitable for complex vehicle design problems. Oh et al. [6] developed a subframe using a hydraulic forming technology. To improve the stiffness of the suspension and reduce the maximum stress that affects the durability cycle life, they adopted a variety of optimization design techniques, shape, size, and topology optimization, and formed the shape of the optimized rear suspension through a hydraulic forming process. The effectiveness of this design method was proven by finite element commercial software. To improve the NVH performance of vehicles, Park et al. [7] studied the front subframe of the vehicle, optimized the dynamic stiffness of the suspension bushing of the subframe, analysed the advantages and disadvantages of the integral subframe with different total shapes, and proposed structural reinforcement and other methods to improve the overall NVH performance of the vehicle. Hur and Lee [8] designed an integrated method for pre-tests, modelled associations and updated analyses of automobile subframes, evaluated model correlations by combining modal parameters of modal tests and finite element analyses, and analysed changes in the natural frequencies and MAC values of material characteristics based on sensitivity analysis results. The iterative method was used to modify the finite element model, and good results were obtained. Belingardi et al. [9] established the goals of strength, stiffness, and natural frequency of the subframe. The subframe designed using composite materials and optimizing the placement of stiffeners was superior to the steel subframe. Chiu Huang [10] designed a hydraulic moulding mould for the subframe, which could be used to achieve a lightweight subframe design. Han et al. [11] applied composite materials to the chassis component subframe, comparing the natural frequency and damping characteristics of steel and composite test pieces, achieving a certain improvement in stiffness, strength, and NVH performance of the composite subframe compared to the steel subframe, achieving a 50% weight reduction effect. Law et al. [12] proposed a new design method for the subframe after studying the subframe structure and design methods. The subframe structure designed using this method was superior in terms of lightness of weight and durability. Jang et al. [13] conducted a lightweight optimization design for the front subframe structure of a car. After optimization, while ensuring performance indicators, the optimized front subframe mass decreased by 30%, while verifying the practicality of the optimization design method. Fichera et al. [14] conducted theoretical calculation and analysis of the performance and load of the subframe, and then conducted topology optimization on the subframe structure, which resulted in a reasonable subframe structure. Rotondella et al. [15] constructed a subframe welding model and verified the reliability of the model through comparison of experiments and simulations. This method could predict structural dynamic characteristics. Da'Quan et al. [16] used ANSYS to study the topology optimization of the subframe under complex load conditions. The study found that the structural performance of the side member of the subframe was improved, while the weight of the subframe remained unchanged. Price et al. [17] designed a cast aluminium alloy subframe that reduced the weight by 40% while maintaining the same strength as the original subframe by optimizing weight and geometry. Liao et al. [18] designed a new high-strength steel subframe structure based on the stiffness and strength analysis of the subframe under

various working conditions. Through comparative analysis of various performances with the original subframe, the feasibility of the new subframe was verified. Hamdi et al. [19] optimized the design of the subframe, which resulted in a significant improvement in NVH performance and a significant reduction in quality. Through verification, this method has made a positive contribution to improving vehicle NVH performance.

In this paper, an aluminium alloy front subframe envelope is first established based on the original steel front subframe, the topology optimization of the aluminium alloy front subframe envelope is carried out by the method of multi-condition topology optimization, and the optimal force path of the subframe is obtained. According to the topology optimization results in CATIA with regards to the detailed mathematical modelling design, its strength, stiffness, and modal performance analysis, the aluminium alloy front subframe performance indicators are obtained. Then, the aluminium alloy front subframe after topology optimization is used to establish a parametric model. Based on the Isight optimization platform, the optimal Latin hypercube test method is used to generate sample points [20], and an approximate response surface model of the aluminium alloy front subframe is constructed. Regarding a former deputy frame optimization design, the multi-objective particle swarm optimization algorithm is adopted for aluminium alloys. Through the analysis of the strength, static stiffness, and modal and fatigue durability, the performance of the aluminium alloy front subframe meets the design requirements, and the modal error of the aluminium alloy front subframe sample and the finite element analysis modal is less than 15%. Moreover, this model successfully passed the bench fatigue durability test.

## 2. Multi-Condition Topology Optimization of the Aluminium Alloy front Subframe

The aluminium alloy front subframe envelope body is established based on the hard points of each subframe connection. The principle of establishing the aluminium alloy front subframe envelope body should ensure that there is no movement interference between the envelope body and the surrounding parts. The established envelope body is shown in Figure 1. The aluminium alloy material used is a ZL114A cast aluminium alloy with a density of  $2.68 \times 10^{-9} \text{ t/mm}^3$ , Poisson's ratio of 0.33, elastic modulus of  $7.24 \times 10^4 \text{ MPa}$ , yield strength of 230 MPa, and tensile strength of 290 MPa.

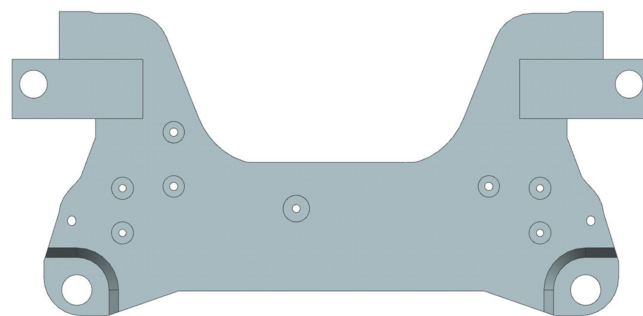


**Figure 1.** Aluminium alloy front subframe envelope.

The subframe will encounter various working conditions during use, so the influence of the various working conditions on the subframe structure should be comprehensively considered in exploitation and design. Regarding vice frames, the typical working conditions are the forward braking condition, backward braking condition, forward emergency braking condition, backward emergency braking condition, overconvex hull condition, over unilateral hull condition, over one side deep pit condition, ultimate steering condition, steering braking condition, steering drive condition, maximum driving acceleration condition, and diagonal torsion condition. The load information of each typical working condition extracted from the multibody dynamics analysis software Adams/car is summarized and used to check the strength of the aluminium alloy front subframe, as shown in Table 1. Due to space limitations, only part of the load information is shown here.

**Table 1.** Summary of load information of each typical working condition.

Load Loading Condition	Load Extraction Position	FX/N	FY/N	FZ/N	TX/N.mm	TY/N.mm	TZ/N.mm	
Forward braking		3284.07	−13,698.91	976.43	−12,565.55	−4972.73	17,758.18	
Backward braking		−1938.66	5250.36	440.28	2433.93	7908.52	−17,822.63	
Forward emergency braking		3603.93	−12,297.02	503.65	−10,162.87	−6142.74	17,802.89	
Backward emergency braking	Left front mounting point of lower control arm	−2567.50	5922.08	384.72	1116.05	10,045.76	−19,683.54	
Overconvex hull		−312.96	−2037.32	330.97	−16,806.04	682.42	−1978.72	
Over unilateral hull		−471.74	−3045.79	522.29	−17,978.29	624.39	−2796.88	
Over one side deep pit		2486.79	−19,902.80	3368.50	−19,125.35	−2931.95	18,310.30	
Ultimate steering		160.90	12,037.52	−1142.56	−14,712.09	−395.00	−8286.05	
Steering braking		2172.52	−4666.31	467.00	−13,050.78	−3580.23	14,608.78	
Steering drive		−1786.45	13,389.08	933.28	501.83	8327.25	−22,282.73	
Maximum driving acceleration		−959.99	3711.35	661.49	11,256.40	5734.13	−10,161.87	
Diagonal torsion		−330.45	−2186.29	192.93	−12,220.28	305.09	−2008.30	
Forward braking			6415.23	11,730.02	−399.92	−17,445.81	4444.70	1461.34
Backward braking			−3404.68	−6275.54	−788.88	2620.12	−84.12	−2600.15
Forward emergency braking			7662.75	13,728.38	10.44	−13,110.00	3269.03	2080.89
Backward emergency braking	Left rear mounting point of lower control arm	−5073.90	−8907.96	−945.29	248.28	838.25	−2830.12	
Overconvex hull		−392.48	−749.21	88.65	−28,138.93	7174.87	−3304.56	
Over unilateral hull		−608.28	−1141.71	153.51	−30,776.38	7415.47	−3843.70	
Over one side deep pit		3891.64	7412.00	−1043.45	−32,024.11	6871.48	−588.33	
Ultimate steering		−355.88	−657.69	56.79	−23,436.62	6460.99	−3803.89	
Steering braking		3647.18	7040.50	−319.42	−18,503.06	4927.97	506.97	
Steering drive		−4046.88	−7266.67	−699.38	−772.01	983.45	−3228.57	
Maximum driving acceleration		−1541.12	−2936.89	−705.71	15,925.78	−3253.31	−2182.21	
Diagonal torsion		−439.74	−838.45	42.95	−18,237.10	5292.08	−1926.40	
Forward braking			−35.71	282.71	−42.47	−5.02	−335.09	−5480.94
Backward braking			−37.87	−61.51	−76.32	179.50	−675.91	1313.98
Forward emergency braking			−481.47	250.38	150.66	164.99	−2733.61	−5023.66
Backward emergency braking	Steering gear left mounting point	352.29	−63.17	64.88	217.27	1332.79	1586.27	
Overconvex hull		−89.30	74.38	9.83	166.08	−829.91	−1352.61	
Over unilateral hull		−150.66	−221.96	79.69	−853.46	−1710.82	−1956.74	
Over one side deep pit		502.53	2156.57	−778.59	1839.08	6405.35	−4312.94	
Ultimate steering		349.17	887.21	−328.71	−229.11	4762.88	2935.18	
Steering braking		47.06	633.97	−97.38	−452.64	1676.53	−2247.49	
Steering drive		−730.26	−1058.18	−224.87	−1624.26	−8359.98	2036.35	
Maximum driving acceleration		−290.88	−45.50	−356.40	43.70	−1885.46	733.59	
Diagonal torsion		−98.05	−185.83	−19.56	−1143.84	−1169.12	−1932.29	

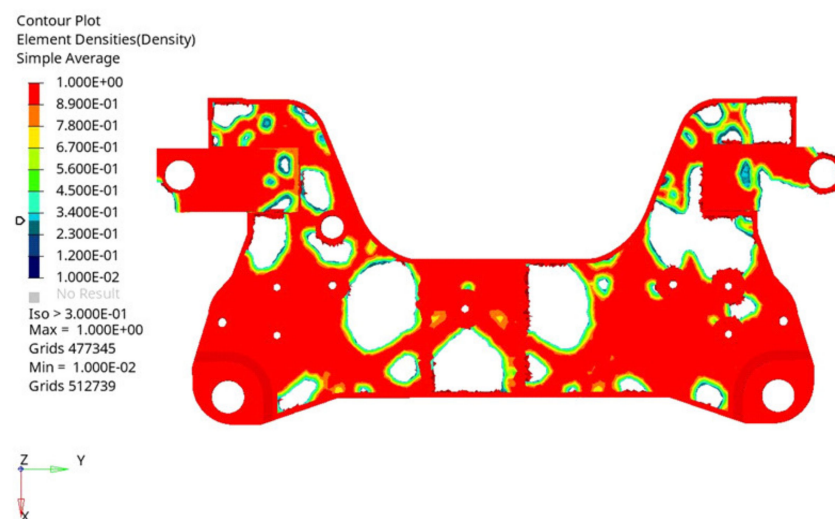
The topology optimization method based on the compromise programming method in Optistruct software is used to optimize the topology of the aluminium alloy front subframe under multiple working conditions. The compromise programming method solves the optimal solution of the multi-objective optimization problem by approximating the one-by-one objective function. It can not only deal with the relative importance of different objective functions, but also give the sensitivity analysis of the optimal strategy to each constraint condition. It can also weigh multiple objectives, avoiding the disadvantage of not considering other influencing factors in the single objective optimization. The volume

percentage and weighted compliance are taken as the optimization response; the goal was to minimize the weighted compliance. The volume percentage is taken as the constraint condition, and the symmetric constraint and the process restriction of the unidirectional drawing die are introduced. Considering the influences of 12 typical working conditions on the topology optimization, the corresponding topology optimization model can be expressed as [11]:

$$\left\{ \begin{array}{l} \min C(\rho) = \left\{ \sum_{k=1}^m w_k^q \left[ \frac{C_k(\rho) - C_k^{\min}}{C_k^{\max} - C_k^{\min}} \right]^q \right\}^{\frac{1}{q}} \\ s.t. \frac{V(\rho)}{V_0} \leq volfrac \\ cons = volfrac \\ geo = symmetry \\ \sigma_{\max} < [\sigma] \end{array} \right. \quad (1)$$

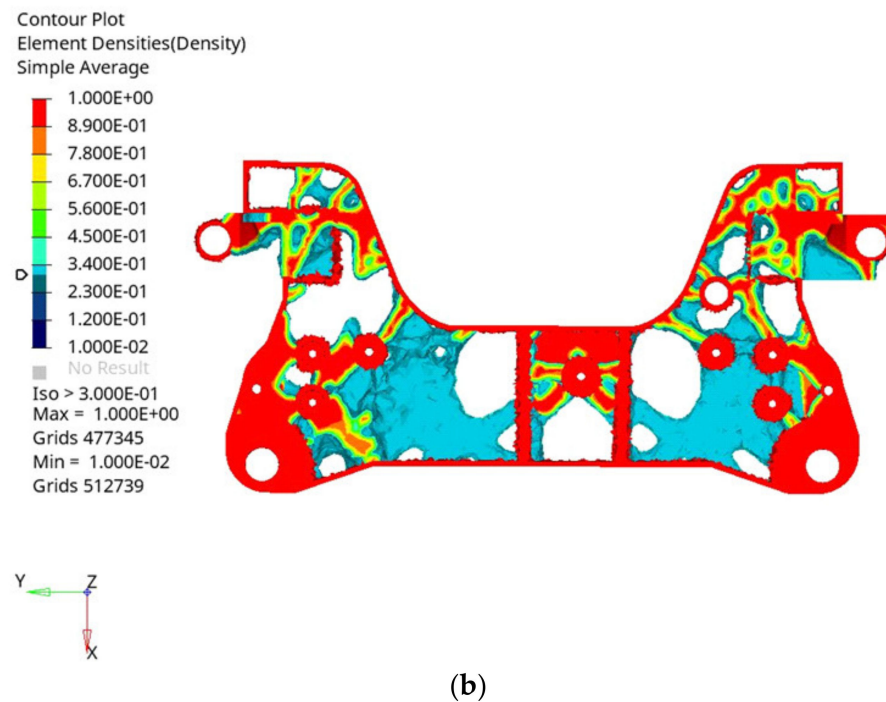
where  $C(\rho)$  is the objective function of comprehensive compliance;  $m$  is the total number of working conditions;  $w_k$  is the weight value in the  $k$ -th working condition;  $C_k(\rho)$  is the objective function of compliance under the  $k$ -th working condition;  $C_k^{\min}$  and  $C_k^{\max}$  are the minimum and maximum compliance values of the  $k$ -th working condition, respectively;  $V(\rho)$  is the volume after topology optimization;  $V_0$  is the volume before topology optimization;  $volfrac$  is the volume percentage;  $cons$  is the constraint condition;  $geo$  is the geometric limit;  $symmetry$  is the symmetric constraint;  $\sigma_{\max}$  is the maximum stress under the ultimate load condition; and  $[\sigma]$  is the allowable stress of the material.

By dividing the aluminium alloy front subframe envelope into the design area and the non-design area, the minimum and maximum member sizes are set. The minimum member size should be more than 3 times the average mesh size of the model, and the maximum member size should be more than 2 times the minimum member size, in order to eliminate the excessive concentration of materials. Because the aluminium alloy front subframe envelope mesh size is 5 mm, here the minimum member size is set to 16 and the maximum member size is set to 40. After 21 iterations, the topology optimization results of the aluminium alloy front subframe envelope obtained when the threshold is adjusted to 0.3 are shown in Figure 2.



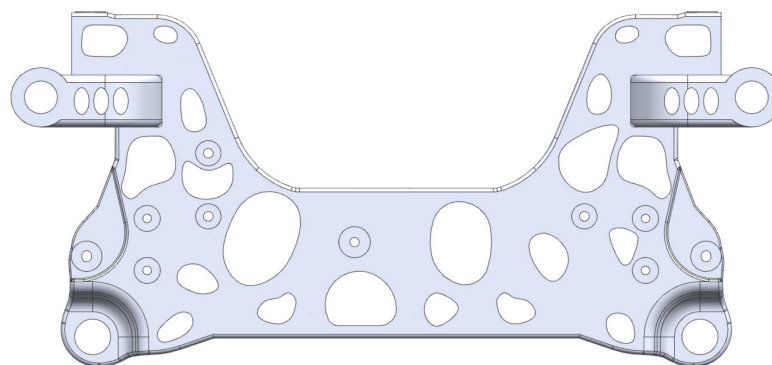
(a)

Figure 2. Cont.



**Figure 2.** Topology optimization results of aluminium alloy front subframe envelope under multiple working conditions. (a) Positive results of multi-condition topology optimization. (b) Rear result of multi-condition topology optimization.

Based on the topology optimization results, according to the stress path of the aluminium alloy front subframe envelope and considering the position of the reinforcing bars, the detailed digital modelling design of the aluminium alloy front subframe is carried out in CATIA. The detailed design digital modelling of the aluminium alloy front subframe is shown in Figure 3. The weighing result of the aluminium alloy front subframe in CATIA is 18.55 kg.



**Figure 3.** Aluminium alloy front subframe detailed design of digital model.

### 3. Performance Analysis of the Aluminium Alloy Front Subframe

#### 3.1. Strength Performance Analysis of the Aluminium Alloy Front Subframe

The strength performance of the aluminium alloy front subframe under each typical working condition is analysed according to the typical working condition load extracted by multibody dynamics. The establishment of displacement and load boundary conditions for the aluminium alloy front subframe is shown in Figure 4.

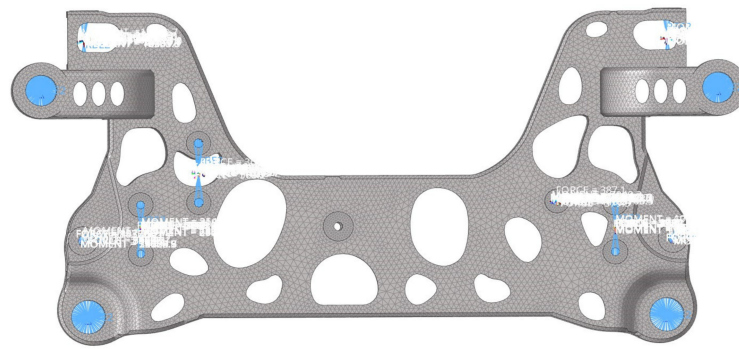


**Figure 4.** Establishment of displacement and load boundary conditions for aluminium alloy front subframe.

The analysis results are shown in Figure 5. Due to space limitations, only part of the stress analysis results of the aluminium alloy front subframe under typical working conditions are listed. According to the cloud diagram of the stress analysis results, it can be seen that the stress of the aluminium alloy front subframe under each typical working condition is the maximum when the aluminium alloy front subframe is under the one side deep pit condition. Moreover, the stress value is 180.6 MPa, which is far less than the material yield strength of 230 MPa and is within the safe range of the material. This shows that the aluminium alloy front subframe meets the strength performance requirements and has a large space for optimization.

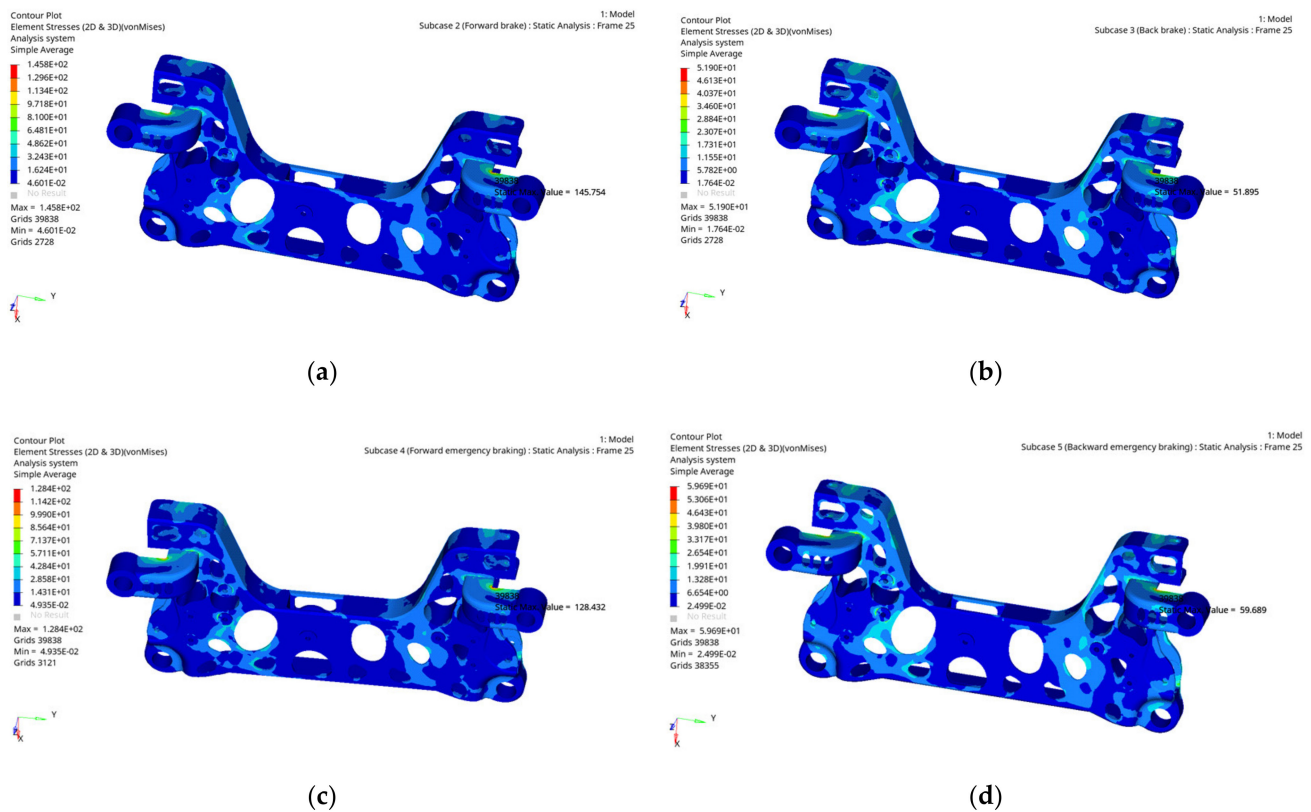


**Figure 5.** Cont.

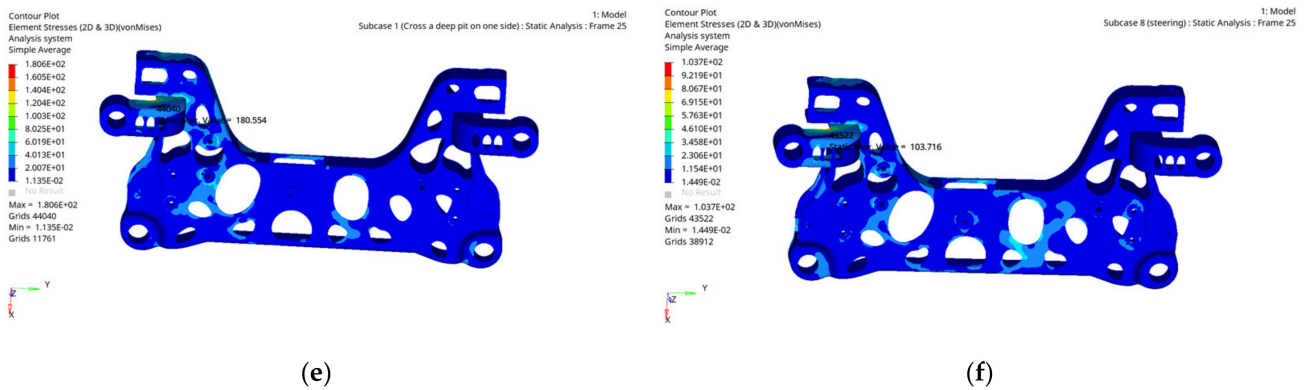


**Figure 5.** Cloud diagram of stress results of aluminium alloy front subframe under some typical working conditions. (a) Forward braking condition. (b) Backward braking condition. (c) Forward emergency braking condition. (d) Backward emergency braking condition. (e) Over one side deep pit condition. (f) Ultimate steering condition.

### 3.2. Static Stiffness Performance Analysis of the Aluminium Alloy Front Subframe

As a bearing part, the aluminium alloy front subframe needs to meet certain static stiffness requirements. Thus, it is necessary to carry out static stiffness analysis on the aluminium alloy front subframe. The static stiffness can be calculated with the ratio of the load of the subframe to the deformation under the corresponding load, as shown in Equation (2):

$$K = \frac{F}{L} \tag{2}$$

where  $K$  is the static stiffness value of the subframe,  $F$  is the load of the subframe at each connection hard point, and  $L$  is the deformation amount under the corresponding load.

In the static stiffness analysis of the aluminium alloy front subframe, the three translational degrees of freedom and three rotational degrees of freedom of the connection position between the aluminium alloy front subframe and the body are constrained. The load condition is a unit force of 1000 N in each of the three translational directions being applied to each installation point of the aluminium alloy front subframe. Table 2 summarizes the static stiffness analysis results at each mounting point of the aluminium alloy front subframe.

**Table 2.** Static stiffness analysis results of each mounting point of the aluminium alloy front subframe.

Number	Position of Mounting Point	Direction	Static Stiffness Value (N/mm)	Target Static Stiffness Value (N/mm)
1	Lower arm left front point	X	23,810	12,000
		Y	25,641	16,000
		Z	40,000	5000
2	Lower swing arm left back point	X	50,000	20,000
		Y	90,909	20,000
		Z	52,631	5000
3	Lower arm right front point	X	13,889	12,000
		Y	45,455	16,000
		Z	45,455	5000
4	Lower swing arm right back point	X	200,000	20,000
		Y	200,000	20,000
		Z	62,500	5000
5	Steering gear left point	X	40,000	25,000
		Y	55,556	25,000
		Z	22,727	8000

Table 2. Cont.

Number	Position of Mounting Point	Direction	Static Stiffness Value (N/mm)	Target Static Stiffness Value (N/mm)
6	Steering gear right point	X	71,429	25,000
		Y	90,909	25,000
		Z	28,571	8000
7	Stabilizer bar left point	X	58,824	10,000
		Y	76,923	5000
		Z	40,000	16,000
8	Stabilizer bar right point	X	100,000	10,000
		Y	111,111	5000
		Z	47,619	16,000

According to the static stiffness analysis results of each installation point, the static stiffness of the aluminium alloy front subframe at each installation point reaches and exceeds the target value.

### 3.3. Free Modal Analysis of the Aluminium Alloy Front Subframe

The natural frequency is a characteristic property of objects. Resonance occurs when externally applied vibrations coincide with the natural frequency of the object. When resonance occurs, vibration and noise will increase dramatically and eventually lead to the destruction of parts [11]. Because the low-order mode has a great influence on the vibration performance of the subframe, usually only the influence of the low-order mode on the subframe is considered. When the vibration frequency of the subframe is close to the excitation frequency, the damage of the parts will be accelerated. Therefore, the frequency of the subframe is close to the excitation frequency, and the frequency of the first-order modal should be increased as much as possible. The modal calculation of the aluminium alloy front subframe is carried out under the OptiStruct module of HyperMesh. The Lanczos algorithm is used to analyse the free modal of the aluminium alloy front subframe. The Lanczos method has a fast convergence speed. The first 6 modals are rigid body modals, so only the modals after the 7th order are considered. To clearly see the modal shape of the subframe, the scaling coefficient is set to 3. The first 6 orders of nonrigid body modal shapes are shown in Figure 6.

The subframe is mainly affected by the ground excitation frequency and engine excitation frequency, while the excitation frequency of general highway pavement is below 25 Hz, and the engine excitation frequency can be calculated by the following formula:

$$f = \frac{n \cdot z}{120} \quad (3)$$

where  $n$  is the idle speed of the engine, r/min, and  $z$  is the number of cylinders of the engine.

The idle speed of the engine of the model under study is 1500 r/min, and the engine is a four-cylinder engine. Thus, the engine excitation frequency is calculated to be 50 Hz, and the free modal of the aluminium alloy subframe should be beyond 50 Hz to avoid resonance. The results of the finite element analysis show that the free modal first-order frequency of the aluminium alloy subframe is 97 Hz. It is much higher than the ground and engine excitation frequency, and the difference between each modal frequency is more than 20 Hz. Thus, the aluminium alloy subframe will not resonate with the excitation frequency, and the modal performance of the aluminium alloy subframe meets the design requirements.

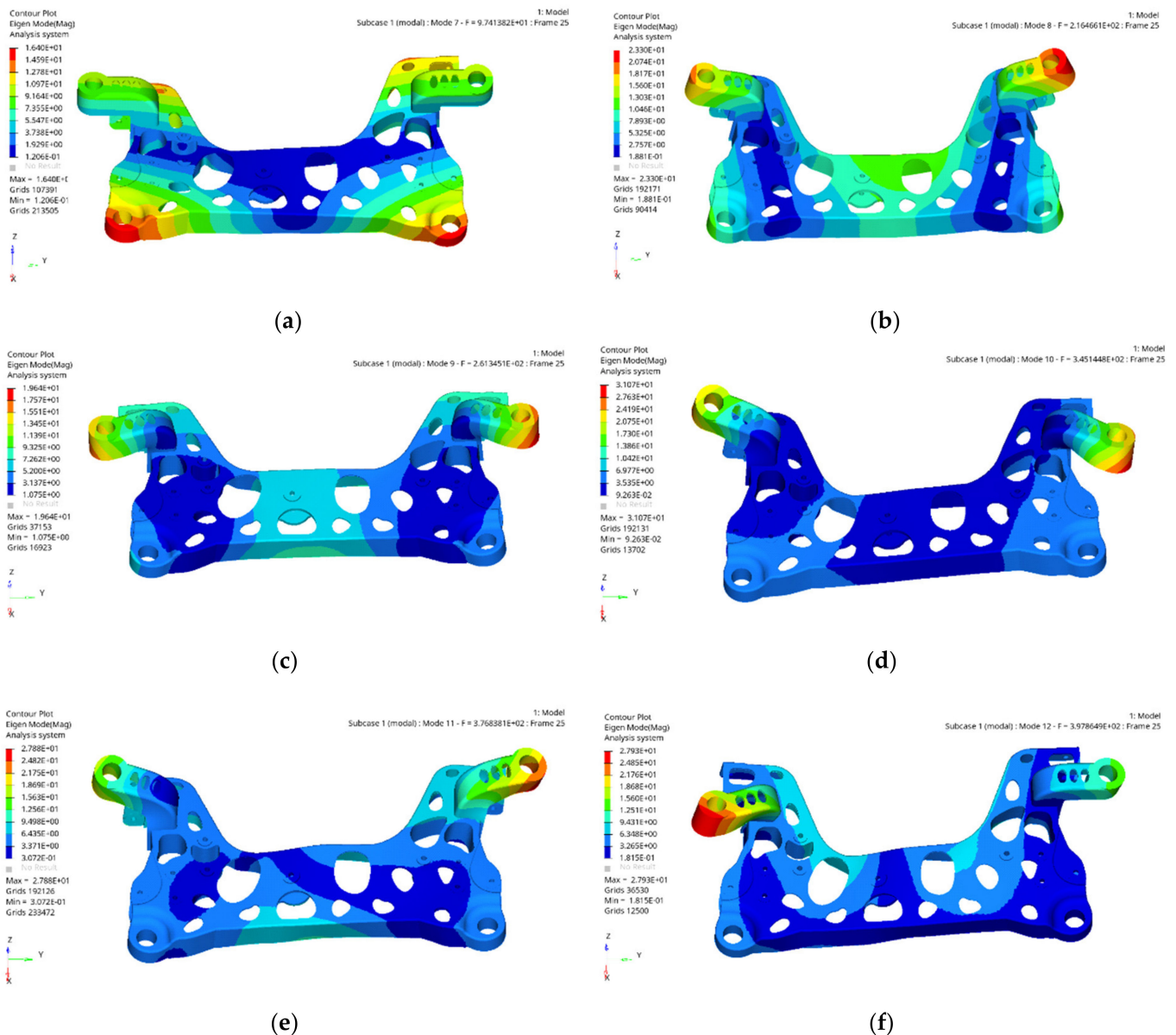


**Figure 6.** Non-rigid body modal shapes for the front 6th order of aluminium alloy front subframe. (a) First order modal shape. (b) Second order modal shape. (c) Third modal shape. (d) Fourth modal shape. (e) Fifth modal shape. (f) Sixth modal shape.

#### 4. Lightweight Optimization Design Based on Multi-Objective Methods

##### 4.1. Establishment of the Parametric Model of the Aluminium Alloy Front Subframe

The parametric model of the aluminium alloy front subframe is created in the Morph module of Ansa. The Morph module can quickly carry out mesh deformation and create shape design variables. Four positions of the aluminium alloy front subframe are selected to set the parametric variables. The parameterized model and optimized positions are shown in Figure 7. The four positions are named F\_01, R\_01, LZ\_t, and LZ\_b. The variation range of the parameterized variables at four positions of the aluminium alloy front subframe is shown in Table 3.

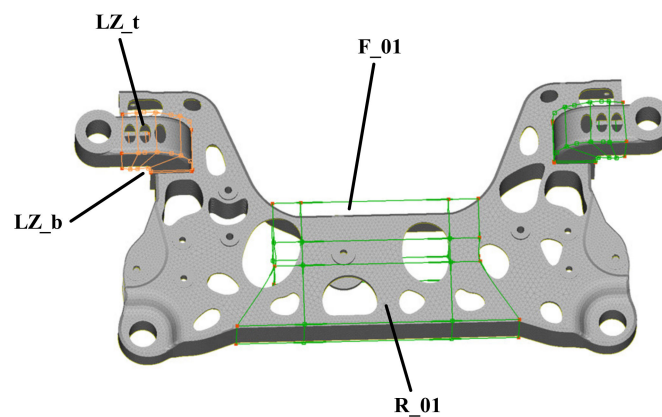


**Figure 7.** Parameterized model and optimized position of aluminium alloy front subframe.

**Table 3.** Variation range of design variables of aluminium alloy front subframe.

Design Variable	Initial Value (mm)	Lower Limiting Value (mm)	Upper Limit Value (mm)
F_01	0	−20	10
R_01	0	−30	15
LZ_t	0	−5	5
LZ_b	0	−8	0

#### 4.2. Establishment of the Optimization Mathematical Model

Based on the strength performance obtained in Section 3.1 and the performance of the modal analysis obtained in Section 3.3, the aluminium alloy front subframe can be further optimized, and the mass can be further reduced. The design of the aluminium alloy front subframe should meet various performance requirements at the same time, including the strength, static stiffness, modal performance, and fatigue endurance performance [18], which is a multi-objective optimization problem [21]. The establishment of a multi-objective optimization design mainly includes the determination of the design variables, constraints, and optimization objectives, as well as the selection of an optimization algorithm. In this paper, the multi-objective optimization platform Isight, combined with Ansa, OptiStruct, and Meta, is adopted to conduct the multi-objective optimization of the aluminium alloy front subframe. The parameters of the aluminium alloy front subframe model were established in the morph module of Ansa; the strength, stiffness, and modal were calculated in the OptiStruct module; and the strength, stiffness, and modal values were extracted in the Meta software. The specific mathematical model is as follows:

$$\text{Object} : \{Mass_{\min}(X) \leq 18, Freq_{1\max}(X), Disp_{\min}(X)\} \quad (4)$$

$$s.t. \begin{cases} 97 \leq Freq_1 \leq 200 \\ Max\_stress1 \leq 180 \\ Max\_stress2 \leq 145 \\ Max\_stress3 \leq 128 \\ Disp_{\min}(X) \leq 0.07 \end{cases} \quad (5)$$

$$\text{Variable} : \begin{cases} -20 \leq F_01 \leq 10 \\ -8 \leq LZ_b \leq 0 \\ -5 \leq LZ_t \leq 5 \\ -30 \leq R_01 \leq 15 \end{cases} \quad (6)$$

where  $Mass_{\min}(X)$  is the minimum mass of the aluminium alloy front subframe;  $Freq_{1\max}(X)$  is the first order frequency of the nonrigid body modal of the aluminium alloy front subframe;  $Disp_{\min}(X)$  is the minimum maximum displacement;  $Freq_1$  is the first order nonrigid body

modal of the aluminium alloy front subframe,  $Max\_stress1$ ,  $Max\_stress2$ ,  $Max\_stress3$  are the stress values of the over one side deep pit condition, forward braking condition, and forward emergency braking condition, respectively; and  $F\_01$ ,  $R\_01$ ,  $LZ\_t$ ,  $LZ\_b$  are the four defined optimization design variables.

4.3. Experimental Design and Establishment of the Approximate Model

Through experimental design, key test factors of the aluminium alloy front subframe can be quickly identified, the optimal combination of the variables and parameters can be identified, and the relationship between the variables and optimization objectives can be analysed to reduce the subjectivity of the design and improve the reliability of the design [22]. In this paper, the optimal Latin hypercube experimental design algorithm is adopted [23,24]. It can make the fitting of factors and responses more accurate and make the sampling points more uniform. The distribution of the optimal Latin hypercube sample points is shown in Figure 8. The number of DOE design points is 25. Figure 9 shows the DOE multi-objective optimization platform built based on Isight.

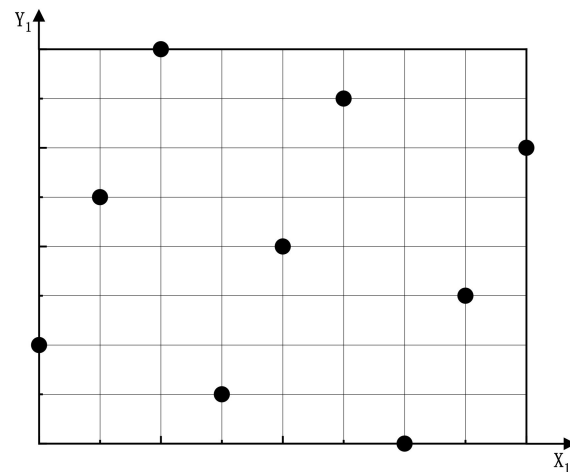


Figure 8. Distribution of optimal Latin hypercube sample points.

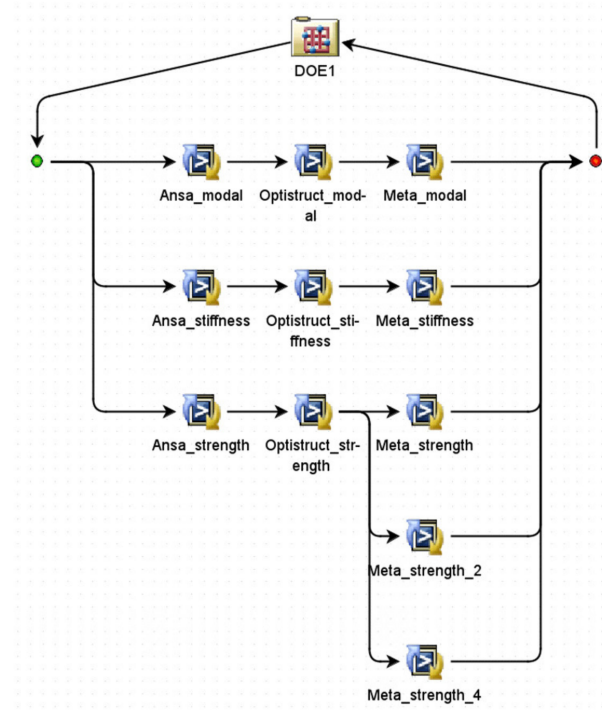


Figure 9. Multi-objective experimental design optimization platform.

DOE1 is the experimental design module; the Ansa\_modal branch is the modal optimization branch, the Ansa\_stiffness branch is the static stiffness optimization branch, and the Ansa\_strength is the strength optimization branch. Regarding the strength optimization, three working conditions with maximum stresses are considered. They are the over one side deep pit condition, forward braking condition, and forward emergency braking condition.

The approximate model method is a method used to approximate a set of input variables and output variables by the mathematical model method. The relationship between the input variables and output response of the approximate model is as follows:

$$y(x) = \tilde{y}(x) + \varepsilon \quad (7)$$

where  $y(x)$  is the actual response value and an unknown function;  $\tilde{y}(x)$  is the response approximation with a known polynomial; and  $\varepsilon$  is the error between the actual value and the approximate value.

When the approximate model has a sufficient accuracy, the approximate model can be used to replace the actual model for simulation analyses to shorten the calculation time and improve the calculation efficiency. Figure 10 shows the construction process of the aluminium alloy front subframe approximate model.

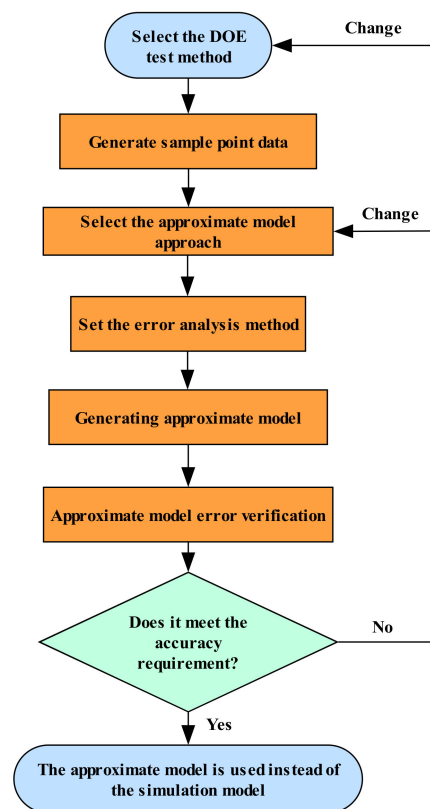


**Figure 10.** Process of building approximate model of aluminium alloy front subframe.

A response surface model is used to construct approximate models [25–27]. Because four positions of the aluminium alloy front subframe are defined as parametric design variables, a second-order polynomial is selected to establish the response surface approximation model, and the specific formula is as follows [28]:

$$\tilde{y} = \beta_0 + \beta_1 x_1 + \beta_2 x_2 + \cdots + \beta_M x_M + \beta_{M+1} x_1^2 + \beta_{M+2} x_2^2 + \cdots + \beta_{2M} x_2 M^2 + \sum_{i \neq j} \beta_{ij} x_i x_j \quad (8)$$

where  $\tilde{y}$  is the response approximation;  $\beta_0, \beta_1, \beta_2 \cdots \beta_M \cdots \beta_{ij}$  are the polynomial coefficients; and  $x_1, x_2 \cdots x_M \cdots x_i$  are the components of the design variable.

After the approximate model is constructed, an error test should be conducted on the fitting results of the approximate model, and the R-squared error analysis method should be used to test the fitting accuracy between the approximate model and the actual sample points [29–31]. The closer R-squared is to 1, the higher the accuracy of the approximate model, with a high credibility. Moreover, a fitting accuracy above 0.9 is generally acceptable. The R-squared value of each response of the aluminium alloy front subframe is shown in Table 4, and it can be seen from Table 4 that the fitting accuracy of each response is greater than 0.98, indicating that the fitting effect of each response variable is good. An approximation model can be used in place of the actual model for multi-objective optimization simulations, thus greatly shortening the computing workload and calculation time.

**Table 4.** Fitted R-squared values for each response.

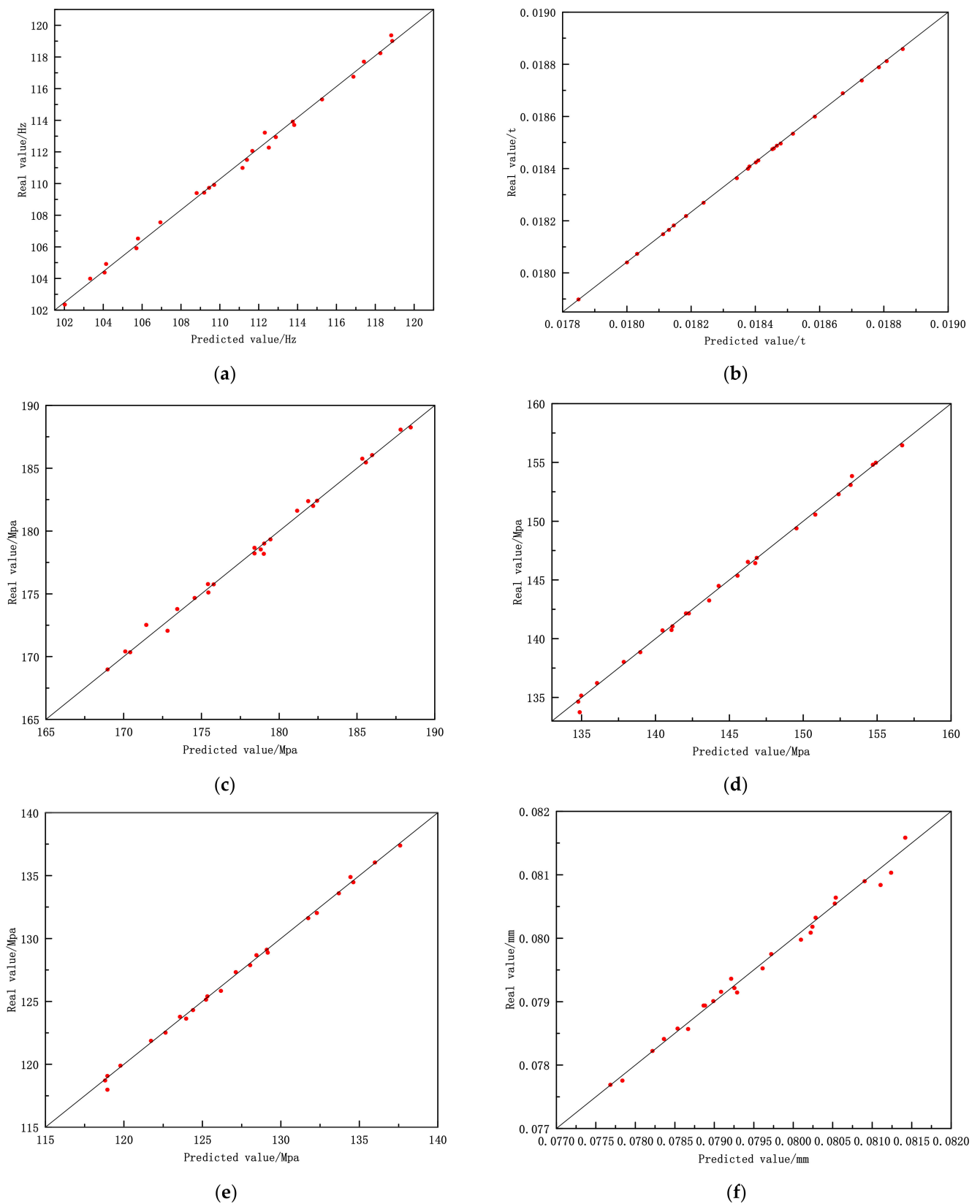
Responses	Total Error
Freq_1	0.99675
Mass	0.99995
Max_stress1	0.99493
Max_stress2	0.99783
Max_stress3	0.99781
Disp	0.9897

Figure 11 shows the fitting results of the predicted and actual values of each response of the aluminium alloy front subframe. The abscissa is the predicted value, and the ordinate is the actual value. The points on the 45° oblique line indicate that the predicted results are the same as the actual results.

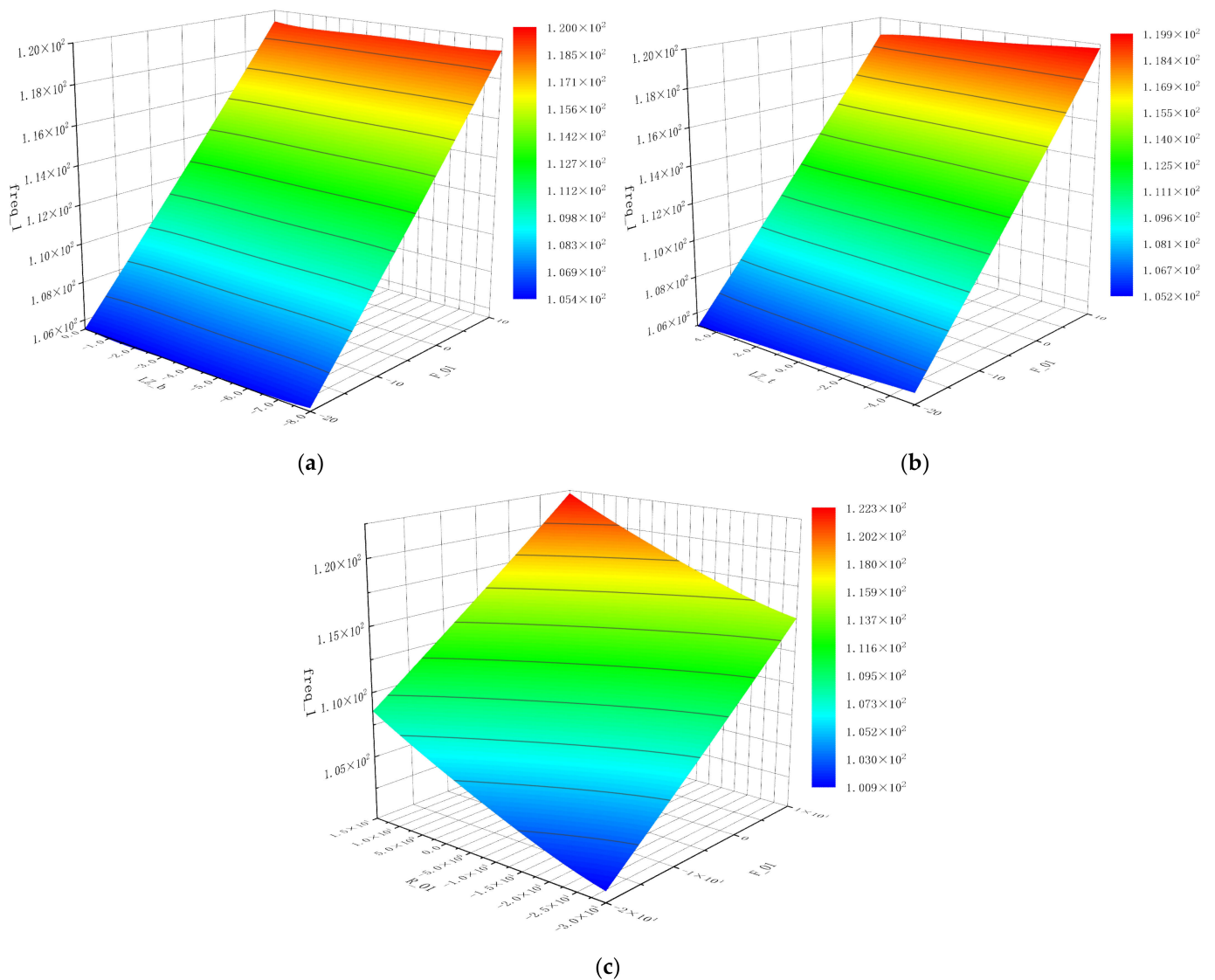
Figure 12 shows the response surface approximation model between the first-order frequency response of the aluminium alloy front subframe and each variable, and the response surface can better express the changing trend of the test point. The corresponding response value of the two variables can be found at any value within the design range. It can be seen from the equal potential surface that the degree of linearity of the fitting is relatively high.

#### 4.4. Multi-Objective Optimization of the Aluminium Alloy Front Subframe Based on the Approximate Model

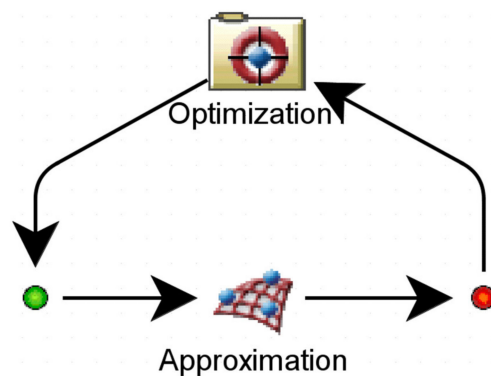
The multi-objective particle swarm optimization algorithm [32] was used to optimize the aluminium alloy front subframe. Multi objective particle swarm optimization is a population-based search process that uses the principles of evolutionary computation: first, initialize from a group of random populations, and search for the optimal value through updating the population generations. The evolution process depends on the previous population. Compared to other optimization algorithms, the advantage of the Multi Objective Particle Swarm optimization algorithm is its strong versatility, simplicity, and ease of implementation, with fewer parameters to adjust. Figure 13 shows the multi-objective optimization design platform based on the approximate model, in which Optimization is the multi-objective optimization module. Moreover, Approximation is the approximate model obtained after generating sample points through the optimal Latin hypercube experimental design. The parameters of the multi-objective particle swarm optimization algorithm are as follows: the maximum number of iterations is set to 100, in order to obtain more optimization results; the number of particles is set to 10; the inertia weight is set to 0.9; the global increment is set to 0.9; the particle increment is set to 0.9; the maximum velocity is set to 0.1; the max failed runs is set to 5; the failed run penalty value is set to  $1.0 \times 10^{30}$ ; the failed run objective value is set to  $1.0 \times 10^{30}$ .



**Figure 11.** The fitting results of the predicted and actual response values of the aluminium alloy front subframe. (a) Results of first-order modal frequency fitting. (b) Mass fitting results. (c) Stress fitting results of over one side deep pit condition. (d) Stress fitting results of forward braking condition. (e) Stress fitting results of forward emergency braking condition. (f) Fitting results of the maximum displacement of the right front point of the lower arm.

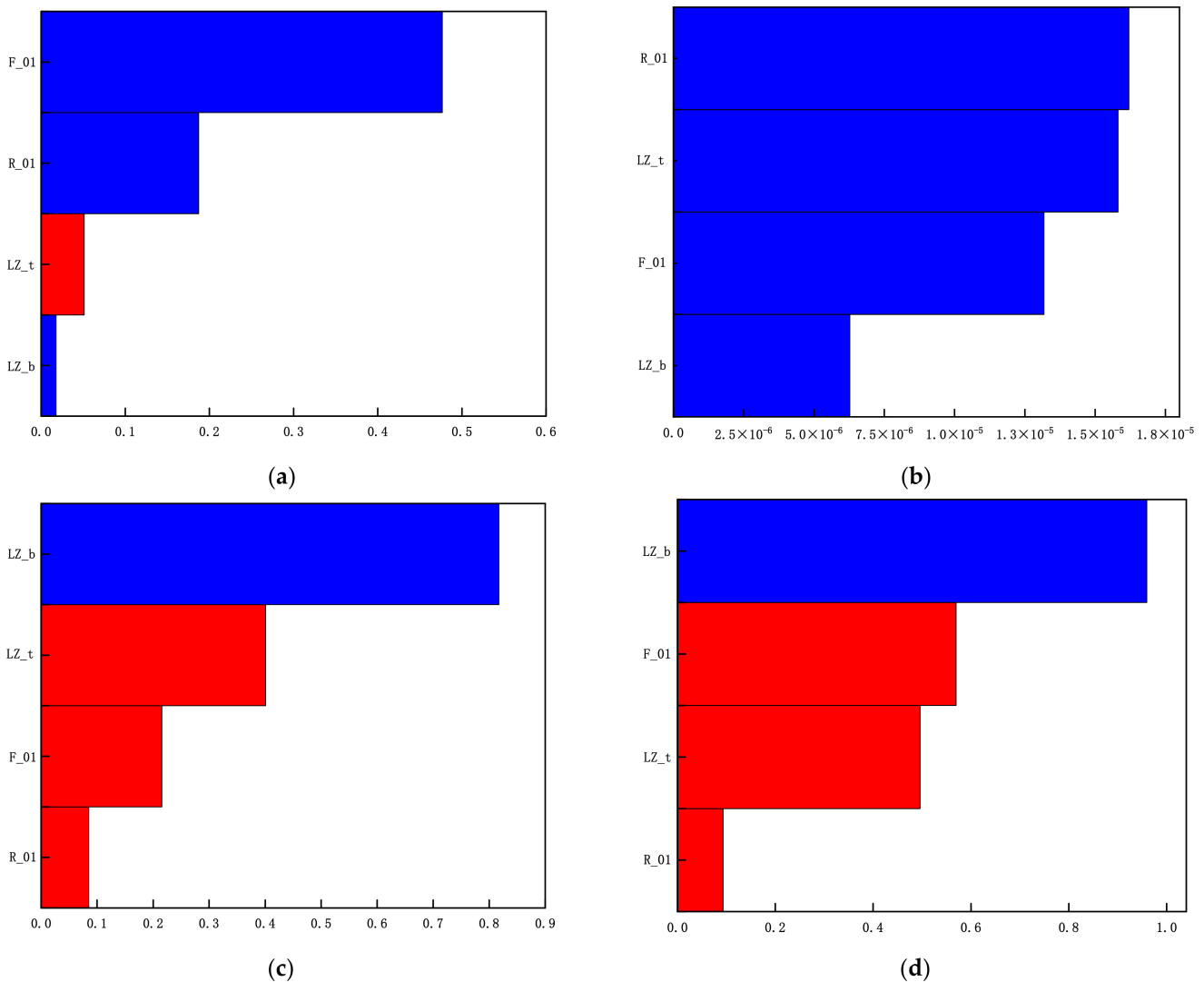


**Figure 12.** First order frequency response and variable response surface approximation model of the aluminium alloy front subframe. (a) Response surface approximation model between the first order frequency of the aluminium alloy front subframe and design variables LZ\_b and F\_01. (b) Response surface approximation model between the first order frequency of the aluminium alloy front subframe and design variables LZ\_t and F\_01. (c) Response surface approximation model between the first-order frequency of the aluminium alloy front subframe and design variables R\_01 and F\_01.



**Figure 13.** Approximate model multi-objective optimization design platform.

The multi-objective optimization design based on the response surface approximation model iteration was run 1002 times. The local effect diagram can show which had the greatest influence on the target response variable and can find the weak link in the design. To better guide the design, the local effect between each variable and the response is shown in Figure 14. Blue represents a positive effect, and red represents a negative effect. From the local effect diagram, it can be seen that F\_01 has the most significant effect on the frequency, R\_01 has the most significant effect on the mass, and LZ\_b has the most significant effect on the stress over one side deep pit condition and forwards braking condition. The optimal solution set was selected from the 1002 iterations to make it closest to the set target value, and the optimal solution of the four variables was finally determined, as shown in Table 5.

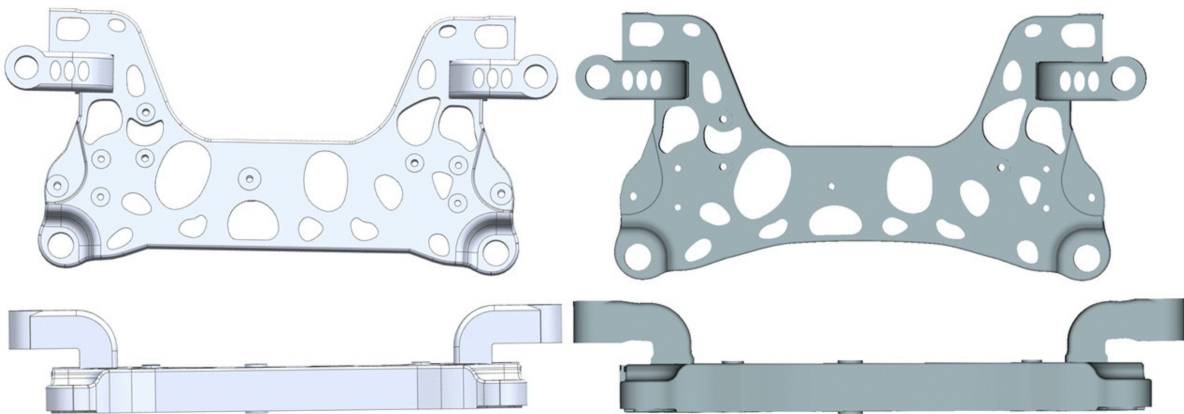


**Figure 14.** Local effect diagram of each variable and response. (a) Frequency local effect diagram. (b) Mass Local Effect diagram. (c) Local effect diagram of stress in over one side deep pit condition. (d) Local effect diagram of forward braking condition.

Figure 15 shows the digital–analogue comparison before and after multi-objective optimization of the aluminium alloy front subframe. After optimization, the weight is reduced from 18.55 kg to 17.6 kg, reducing the weight by 0.95 kg.

**Table 5.** Comparison of variable data before and after optimization.

Design Variable	Initial Value/mm	Lower Limiting Value/mm	Upper Limit Value/mm	Optimal Value/mm
F_01	0	−20	10	1.5
R_01	0	−30	15	−27
LZ_t	0	−5	5	−4
LZ_b	0	−8	0	−4.5

**Figure 15.** Digital and analogue comparison before and after multi-objective optimization of aluminium alloy front subframe.

## 5. Performance Analysis and Verification of the Aluminium Alloy Front Subframe after Optimization

### 5.1. Strength Performance Analysis of the Optimized Aluminium Alloy Front Subframe

The displacement boundary conditions and load boundary conditions from Section 3.1 are used to analyse the strength performance of the optimized aluminium alloy front subframe. Figure 16 shows the cloud diagram of the stress analysis results of the optimized aluminium alloy front subframe under some typical working conditions. According to the cloud diagram of the stress analysis results, the working condition corresponding to the maximum stress of the optimized aluminium alloy front subframe is the limiting condition of the one side deep pit condition, and the stress value is 179.3 MPa, which is 1.3 MPa less than the value of 180.6 MPa before optimization.

Table 6 shows the comparative analysis results of the stress of the aluminium alloy front subframe before and after optimization. After optimization, the stress of the aluminium alloy front subframe is reduced in all typical working conditions, which is less than the material yield strength. After optimization, the aluminium alloy front subframe meets the strength requirements.

**Table 6.** Comparative analysis results of stress before and after optimization of aluminium alloy front subframe.

Typical Working Conditions	Model Stress before Optimization/MPa	Model Stress after Optimization/MPa
Forward braking condition	145.7	141.7
Backward braking condition	51.9	50.2
Forward emergency braking condition	128.4	124.8
Backward emergency braking condition	59.7	57.8
Over one side deep pit condition	180.6	179.3
Ultimate steering condition	103.7	101.9

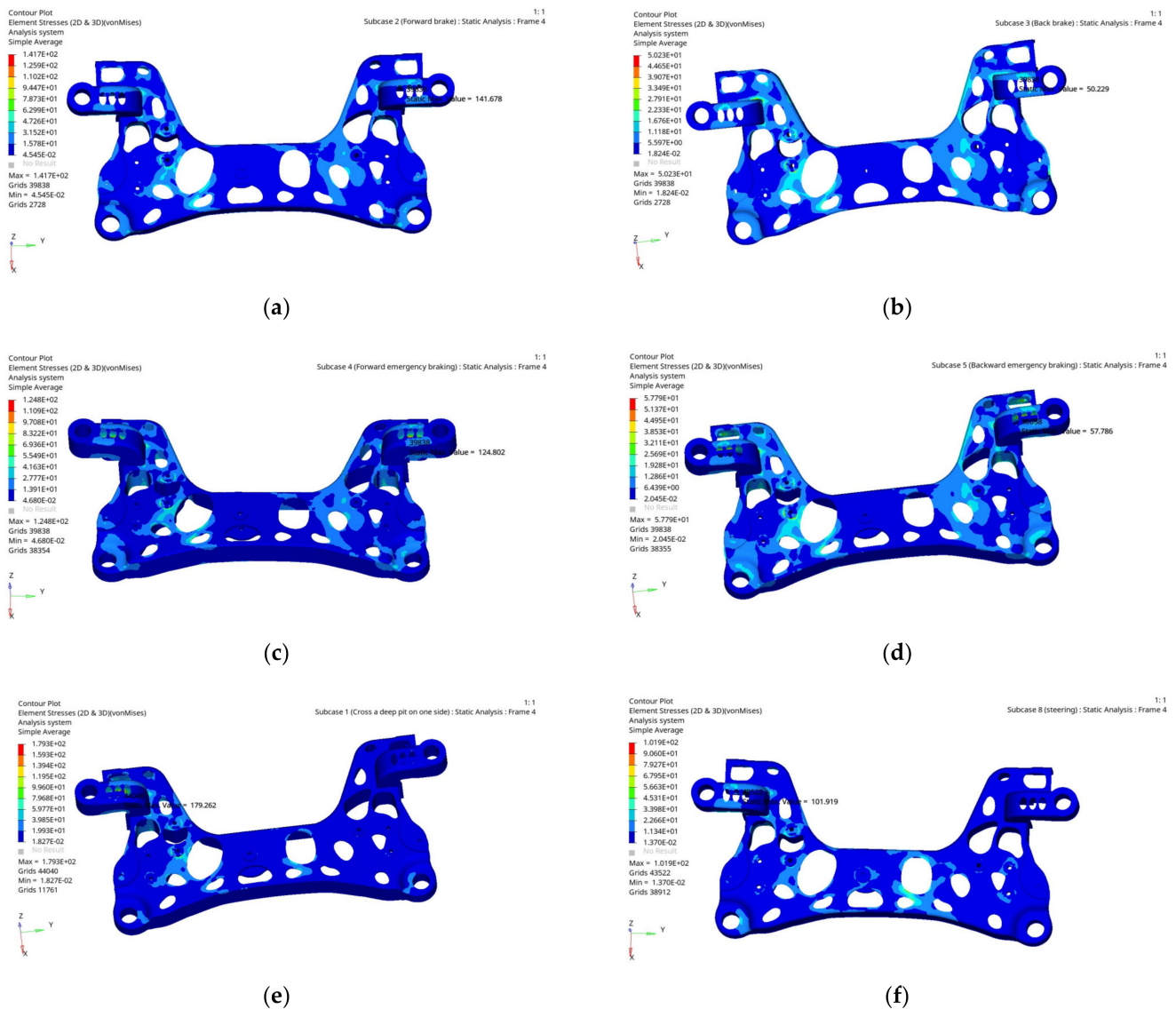


**Figure 16.** Cloud image of stress analysis results of aluminium alloy front subframe under some typical working conditions after optimization. (a) Forward braking condition. (b) Backward braking condition. (c) Forward emergency braking condition. (d) Backward emergency braking condition. (e) Over one side deep pit condition. (f) Ultimate steering condition.

## 5.2. Static Stiffness Performance Analysis of the Optimized Aluminium Alloy Front Subframe

Table 7 shows the comparative analysis results of the static stiffness performance of the aluminium alloy front subframe before and after optimization. The results show that the static stiffness values of each hard point of the aluminium alloy front subframe have little change compared with those before optimization, which is within the acceptable range and meets the design requirements.

## 5.3. Free Modal Performance Analysis of the Optimized Aluminium Alloy Front Subframe

Free modal analysis is carried out on the optimized aluminium alloy front subframe, and the first six rigid body modals are filtered out. The cloud diagram of the free modal analysis results is shown in Figure 17. Table 8 shows the comparison results of the free modal analysis before and after optimization of the aluminium alloy front subframe. After optimization, the first-order modals and fifth-order modals of the aluminium alloy front subframe are slightly reduced, while the other modals are improved. These results are higher than the ground and engine excitation frequencies, and the difference between each

modal frequency is more than 20 Hz. The optimized aluminium alloy front subframe meets the modal performance requirements.

**Table 7.** Comparative analysis results of static stiffness performance of aluminium alloy front subframe before and after optimization.

Number	Position of Mounting Point	Direction	Static Stiffness Value of the Model before Optimization (N/mm)	Static Stiffness Value of Optimized Model (N/mm)
1	Lower arm left front point	X	23,810	24,390
		Y	25,641	23,809
		Z	40,000	37,037
2	Lower swing arm left back point	X	500,000	500,000
		Y	90,909	83,333
		Z	52,631	50,000
3	Lower arm right front point	X	13,889	13,888
		Y	45,455	40,000
		Z	45,455	40,000
4	Lower swing arm right back point	X	200,000	200,000
		Y	200,000	200,000
		Z	62,500	62,500
5	Steering gear left point	X	40,000	38,461
		Y	55,556	52,631
		Z	22,727	21,739
6	Steering gear right point	X	71,429	71,428
		Y	90,909	83,333
		Z	28,571	27,027
7	Stabilizer bar left point	X	58,824	58,823
		Y	76,923	83,333
		Z	40,000	38,461
8	Stabilizer bar right point	X	100,000	100,000
		Y	111,111	111,111
		Z	47,619	45,454

**Table 8.** Comparison of free modal analysis results before and after optimization of aluminium alloy front subframe.

Order	Model Frequency before Optimization/Hz	Optimized Model Frequency/Hz
First order modal	97	96
Second order modal	216	222
Third order modal	261	268
Fourth order modal	345	346
Fifth order modal	376	373
Sixth order modal	397	417

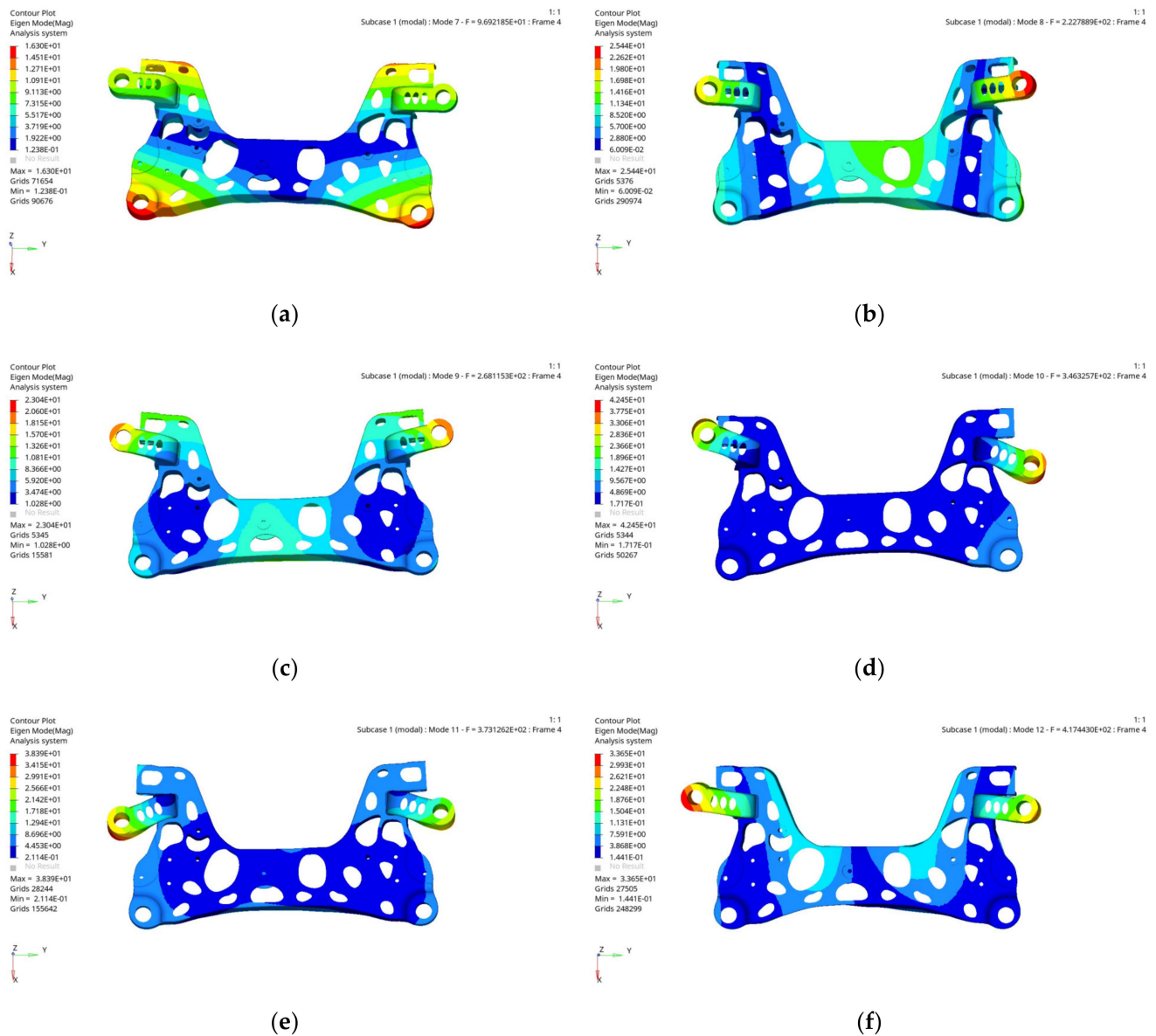


**Figure 17.** Optimized non-rigid body modal shapes for the front 6th order of the aluminium alloy front subframe. (a) First modal shape. (b) Second order modal shapes. (c) Third order modal shapes. (d) Fourth order modal shapes. (e) Fifth order modal shapes. (f) Sixth order modal shapes.

#### 5.4. Fatigue Life Analysis of the Optimized Aluminium Alloy Front Subframe

Automobile parts will be subjected to various excitation loads during use. Even if the automobile parts meet the strength requirements, they will fracture or fail due to fatigue damage. Therefore, it is imperative to carry out a fatigue analysis of the aluminium alloy front subframe. The aluminium alloy front subframe will be affected by the excitation of the ground and the engine during use because of a high stress alternating frequency; therefore, the analysis method of the high cycle fatigue is adopted, that is, the stress-life (S–N) fatigue analysis method [33–37]. The fatigue life analysis of the aluminium alloy front subframe is carried out in the fatigue process module of the HyperMesh software, and the whole fatigue analysis process is shown in Figure 18.

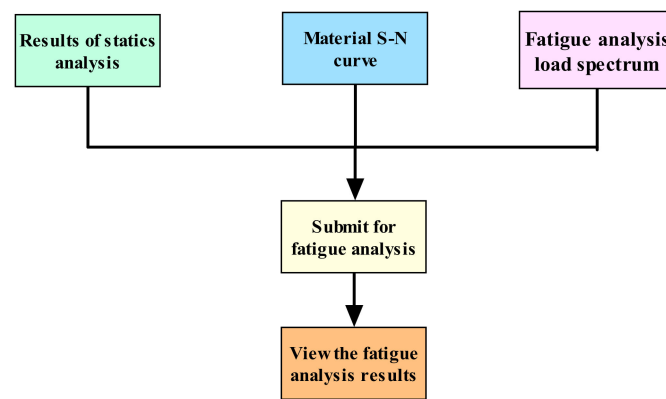


Figure 18. Fatigue analysis flow of aluminium subframe.

After the pre-treatment parameters of the fatigue analysis are set, they are submitted to the solver for calculation. The fatigue life of the aluminium alloy front subframe is analysed under two conditions of high stress: the over one side deep pit condition and forward braking condition. The target value of the fatigue damage is less than 0.25. The fatigue damage cloud diagram and fatigue life cloud diagram of the optimized aluminium alloy front subframe are shown in Figures 19 and 20, respectively, under the one side deep pit conditions.

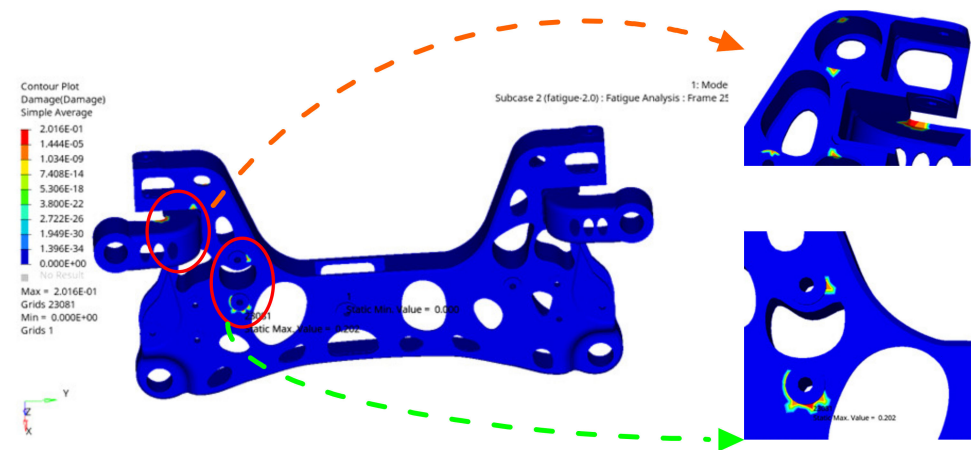


Figure 19. Fatigue damage cloud image of aluminium alloy front subframe over one side deep pit condition.

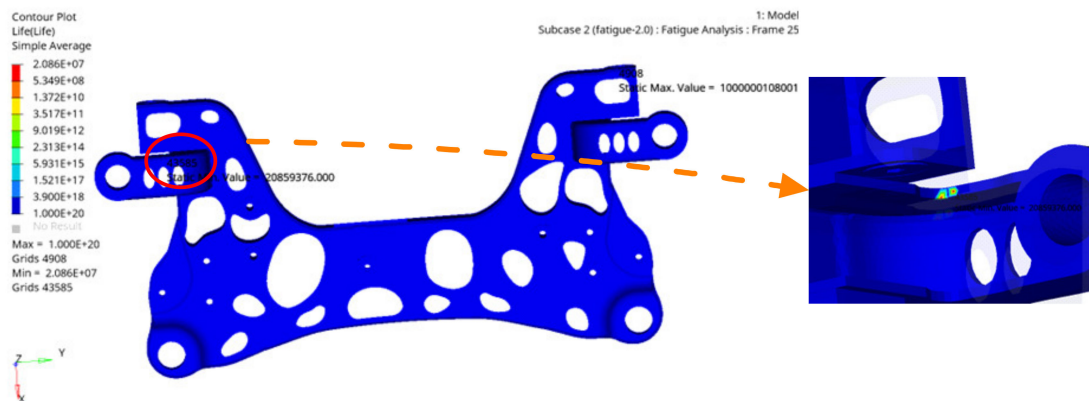
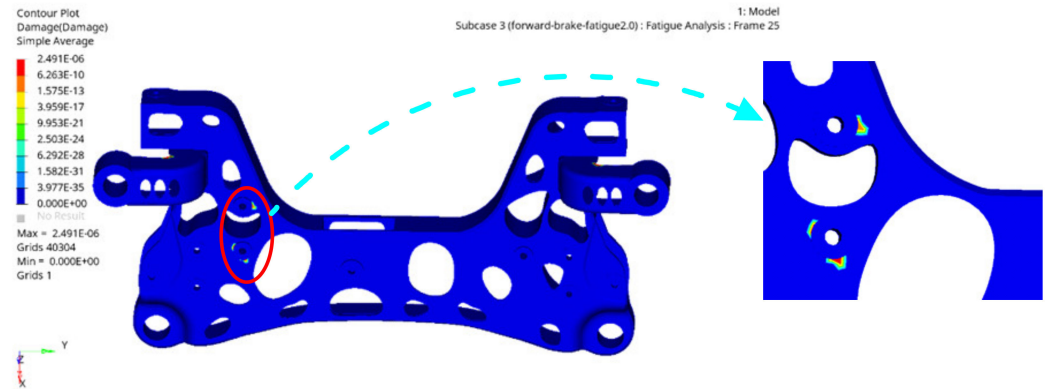


Figure 20. Fatigue life cloud diagram of aluminium alloy front subframe over one side deep pit condition.

It can be seen from Figure 19 that the maximum fatigue damage of the aluminium alloy front subframe is 0.201, which is less than the target value of 0.25; thus, the design requirements are met. It can be seen from Figure 20 that the minimum fatigue life of the aluminium alloy front subframe is  $2.08 \times 10^7$ , which also meets the design requirements.

The fatigue damage cloud diagram and fatigue life cloud diagram of the aluminium alloy front subframe under forwards braking conditions are shown in Figures 21 and 22.



**Figure 21.** Fatigue damage cloud diagram of aluminium alloy front subframe under forward braking condition.

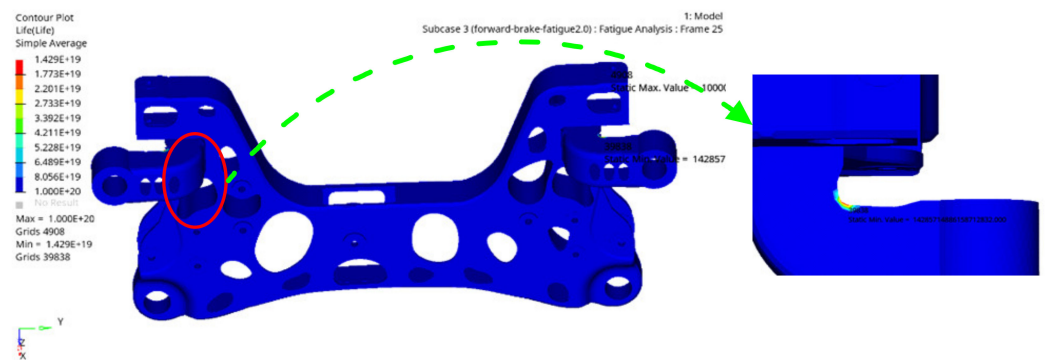


**Figure 22.** Fatigue life cloud diagram of aluminium alloy front subframe under forward braking condition.

Figure 21 shows that the maximum fatigue damage of the aluminium alloy front subframe in the forward braking condition is  $2.49 \times 10^{-6}$ , which is far less than the target value of 0.25; thus, the design requirements are satisfied. Figure 22 shows that the minimum fatigue life of the aluminium alloy front subframe in the forward braking condition is  $1.42 \times 10^{19}$ , which also meets the design requirements.

## 6. Test Analysis of the Aluminium Alloy Front Subframe Sample

### 6.1. Free Modal Test Analysis of the Aluminium Alloy Front Subframe

The aluminium alloy front subframe studied in this paper is produced by an integrated casting method. After casting, the aluminium alloy front subframe sample is obtained by fine machining. To verify the accuracy and reliability of the finite element analysis results, a free modal test of the finished aluminium alloy front subframe was carried out. The modal test equipment used is shown in Figure 23, and the free modal test platform built for the aluminium alloy subframe is shown in Figure 24. The aluminium alloy front subframe sample was suspended on the test bench by a special rubber cord for the modal test so that it was in a free suspension state. The method of force hammer knocking and multipoint picking up was adopted for the modal test [38]. Eight test points were selected in the aluminium alloy front subframe body, and the force hammer knocking position was

repeatedly knocked six times to obtain the average value to improve the accuracy of the test results.

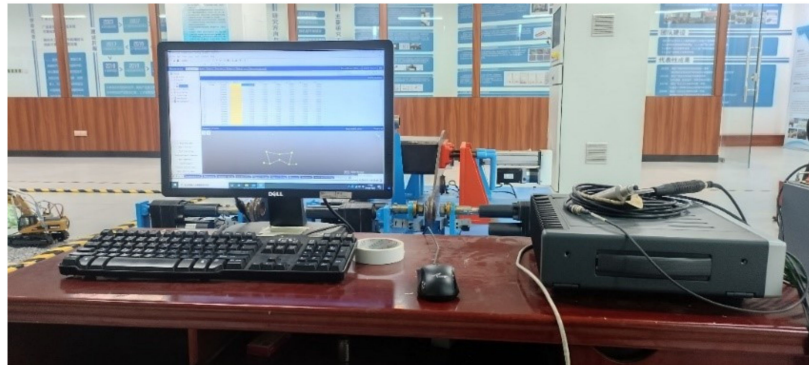


**Figure 23.** Aluminium alloy front subframe modal test equipment.

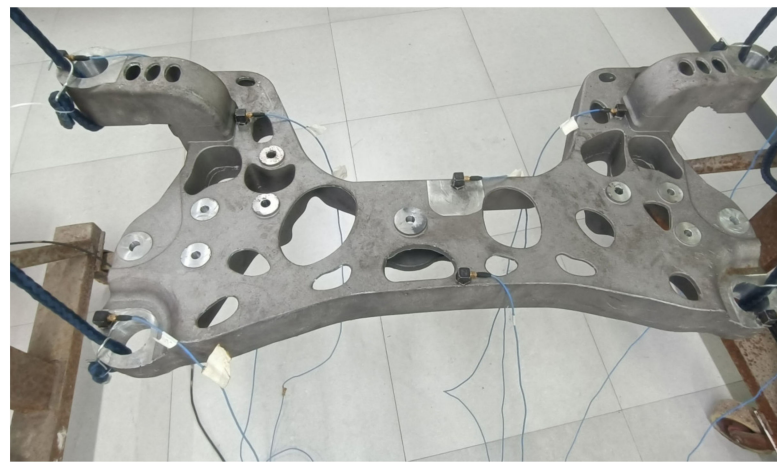


**Figure 24.** Free modal test platform of aluminium alloy subframe.

The least square frequency domain method is used to identify the modal shapes. Figure 25 shows the comprehensive frequency response function curve of the aluminium alloy front subframe. The results show that the first-order modal of the aluminium alloy front subframe is 84 Hz, the second-order modal is 201 Hz, the third-order modal is 254 Hz, the fourth-order modal is 342 Hz, the fifth-order modal is 389 Hz, and the sixth-order modal is 390 Hz. By comparing the free modal finite element analysis results of the aluminium alloy front subframe with the test analysis results, as shown in Table 9, it can be seen that the maximum error of the free modal finite element results and test results of the first six orders of the aluminium alloy front subframe is 14.29%, and the maximum error is no more than 15%, which verifies the accuracy of the finite element model.

**Table 9.** The results of free modal finite element analysis of aluminium alloy front subframe are compared with the results of test analysis.

Order Number	Finite Element Analysis Frequency/Hz	Test Analysis Frequency/Hz	Error/%
First order modal	96	84	14.29
Second order modal	222	201	10.45
Third order modal	268	254	5.93
Fourth order modal	346	342	1.47
Fifth order modal	373	389	1.32
Sixth order modal	417	390	6.92

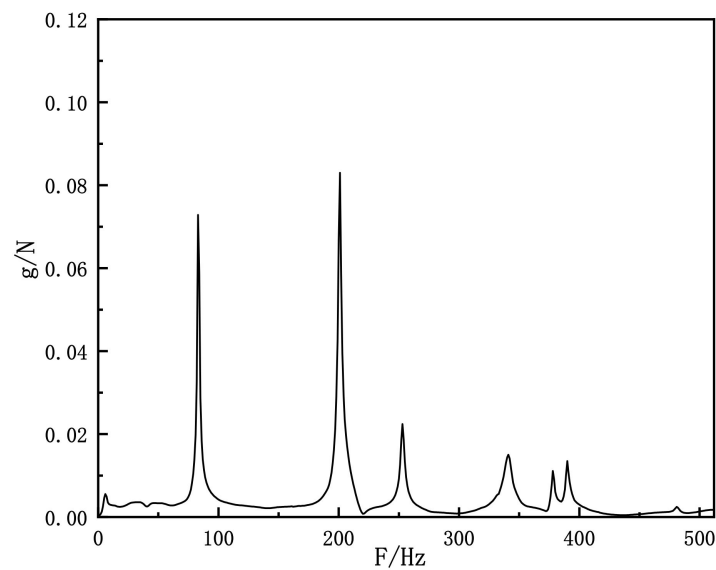


**Figure 25.** Integrated frequency response function curve of aluminium alloy front subframe.

### 6.2. Fatigue Endurance Bench Test of the Aluminium Alloy Front Subframe

To verify the fatigue durability of the front subframe of the aluminium alloy, a fatigue durability bench test was carried out on the front subframe of the aluminium alloy. According to the bench test standards of enterprises, the longitudinal durability test and lateral durability test of the front subframe were investigated, and the durability of the front and rear installation points of the swinging arm of the front subframe of the aluminium alloy was checked. The simulated loading of the aluminium alloy front subframe and the body were bolted together. In the longitudinal endurance test analysis, force values ranging from  $-6$  kN to  $8.6$  kN in the X-direction were loaded on the swing arm ball pin in the form of a sine wave. The test frequency range was  $2$  Hz, and the test target was  $350,000$  times without cracking. The built longitudinal fatigue endurance bench test platform is shown in Figure 26. In the analysis of the lateral force durability test, a force in the direction of  $Y \pm 9$  kN was loaded on the swing arm ball pin in the form of a sine wave. The test frequency range was also  $2$  Hz, and the test target was  $300,000$  times without cracking. The built lateral force fatigue endurance bench test platform is shown in Figure 27.



**Figure 26.** Longitudinal fatigue endurance test of aluminium alloy front subframe on bench.



**Figure 27.** Lateral force fatigue endurance test of aluminium alloy front subframe on bench.

The longitudinal durability test and lateral durability test of the aluminium alloy front subframe verified three samples. It was verified by the test that the aluminium alloy front subframe could reach 350,000 times without cracking in the longitudinal durability test and 300,000 times without cracking in the lateral durability test. These results satisfy the requirements of the bench durability test.

## 7. Conclusions

In this paper, the influence of typical working conditions on an aluminium alloy front subframe structure was considered by the multi-working condition topology optimization method, and the optimal stress path structure of the aluminium alloy front subframe was obtained. According to the optimal stress path structure, the detailed structural design of the aluminium alloy front subframe and the performance analysis showed that the aluminium alloy front subframe met the requirements for the performance of strength, static stiffness, and modal. Further optimization can be obtained. Then, the response surface approximation model was constructed using the optimal Latin hypercube test method Isight. Meanwhile, the multi-objective particle swarm optimization algorithm was used to optimize the multi-objective design of the aluminium alloy front subframe, which further reduced the weight of the aluminium alloy subframe. Aluminium alloy subframe samples were manufactured based on the optimization results. Free modal test analysis and fatigue endurance bench tests were carried out on the aluminium alloy subframe samples. The following conclusions can be drawn from this study.

- The multi-operating condition topology optimization method is adopted to find the best stress path of the aluminium alloy front subframe, which prevents blindness in the design and development process of the aluminium alloy front subframe and can greatly shorten the development cycle.
- The response surface approximation model was constructed by using the optimal Latin Hypercube test method in the Isight software. Meanwhile, the multi-objective particle swarm optimization algorithm was used to carry out the multi-objective optimization design of the aluminium alloy front subframe. After 1002 iterations, the optimal structure of the aluminium alloy front subframe was obtained. After optimization, the maximum stress of the aluminium alloy front subframe corresponds to the extreme single-side pit condition, and the stress value is 179.3 MPa, which is 1.3 MPa less than that of 180.6 MPa before optimization. After optimization, the static stiffness values of each hard point of the aluminium alloy front subframe have little change, while the static stiffness values of some hard points remain unchanged. Under the premise of satisfying various performance indexes, the aluminium alloy front subframe loses 0.95 kg compared with the topology optimization, and 2.4 kg compared with the original subframe, with a lightweight rate of 12%.

- Free modal test analysis was carried out on the aluminium alloy front subframe sample after multi-objective optimizations. The error between the test results and the finite element free modal analysis results was less than 15%, which verified the accuracy of the finite element model. The fatigue endurance bench test of the aluminium alloy front subframe samples showed that the longitudinal endurance test of the aluminium alloy front subframe could reach the target value of 350,000 times, and the lateral endurance test could reach the target value of 300,000 times, satisfying the bench fatigue durability requirements.

**Author Contributions:** Conceptualization, Y.S. and X.M.; methodology, X.M., W.L. and Z.Z.; software, X.M.; validation, Y.S., X.M. and Z.Z.; formal analysis, J.H.; writing—original draft preparation, X.M.; writing—review and editing, Y.S.; funding acquisition, Y.S. All authors have read and agreed to the published version of the manuscript.

**Funding:** This work was supported by the Central Guidance Project of China (ZY21195053) and the Science and Technology Project of Liuzhou (2021CBA0102).

**Data Availability Statement:** All data used to support the findings of this study are included within the article.

**Conflicts of Interest:** The authors declare no conflict of interest.

## References

1. Li, C.; Kim, I.Y.; Jeswiet, J. Conceptual and detailed design of an automotive engine cradle by using topology, shape, and size optimization. *Struct. Multidiscip. Optim.* **2015**, *51*, 547–564. [[CrossRef](#)]
2. Kim, S.I.; Kang, S.W.; Yi, Y.S.; Park, J.; Kim, Y.Y. Topology optimization of vehicle rear suspension mechanisms. *Int. J. Numer. Methods Eng.* **2018**, *113*, 1412–1433. [[CrossRef](#)]
3. Ali, U.; Fraser, R.A. *Numerical Modeling of Rear Subframe under Different Loading Conditions*; 2013-01-0571; SAE 2013 World Congress & Exhibition: Detroit, MI, USA, 2013.
4. Nam, J.; Shin, H.; Choi, G. Durability prediction for automobile aluminum front subframe using nonlinear models in virtual test simulations. *Int. J. Automot. Technol.* **2014**, *15*, 593–601. [[CrossRef](#)]
5. Lee, G.S.; Park, J.M.; Choi, B.L.; Choi, D.H.; Nam, C.H.; Kim, G.H. Multidisciplinary Design Optimization of Vehicle Front Suspension System Using PIDO Technology. *Trans. Korean Soc. Automot. Eng.* **2012**, *20*, 1–8.
6. Oh, J.H.; Choi, H.H.; Park, S.H. The Optimization of Rear Suspension Using Hydroforming. *Trans. Mater. Process.* **2008**, *17*, 481–485.
7. Park, S.Y.; Park, D.C.; Yoon, K.S.; Lee, M.S. *A Study of Front Subframe System Optimization for Improving Vehicle NVH Performance*; 2009-01-2097; SAE 2009 Noise and Vibration Conference and Exhibition: St. Charles, IL, USA, 2009.
8. Hur, D.; Lee, K. A Study on the FE Model Updating and Optimization for Vehicle Subframe. *Trans. KSAE* **2003**, *10*, 220–227.
9. Belingardi, G.; Koricho, E.G. Design of a composite engine support sub-frame to achieve lightweight vehicles. *Int. J. Automot. Compos.* **2014**, *1*, 90–111. [[CrossRef](#)]
10. Chiu, H.; Cheng, K.; Chang, M.; Chi, S. *The Lightweight Chassis Sub-Frame Design by Applying Hydroforming Technology*; 2010-01-0989; SAE 2010 World Congress & Exhibition: Detroit, MI, USA, 2010.
11. Han, D.-H.; Ha, S. Development of lightweight composite sub-frame in automotive chassis parts considering structure & NVH performance. *Compos. Res.* **2019**, *32*, 21–28.
12. Law, S.E.; Widmer, D.R. *Crossmember Design Process—A Case Study*; 2001-01-3068; SAE 2002 World Congress & Exhibition: Detroit, MI, USA, 2001.
13. Jang, C.-S.; Yoo, Y.-D.; Jeon, J.-W.; Choi, B.-L.; Jung, E.-W. *Design of a Light Weight Suspension Component Using CAE*; 980901; International Congress & Exposition: Detroit, MI, USA, 1998.
14. Fichera, G.; Scionti, M.; Petrone, F. Optimization of the mount system of a vehicle's front subframe. *Shock. Vib. Dig.* **2006**, *38*, 342–343.
15. Rotondella, V.; Merulla, A.; Baldini, A.; Mantovani, S. Dynamic modal correlation of an automotive rear subframe, with particular reference to the modelling of welded joints. *Adv. Acoust. Vib.* **2017**, *2017*, 8572674. [[CrossRef](#)]
16. Da'Quan, L.; Zhou, J.; Park, J. The Use of Topology Optimization in Enhancing the Structural Property of an Automotive Front Sub-Frame. In Proceedings of the 2022 ASEE Gulf Southwest Annual Conference, Prairie View, TX, USA, 16–18 March 2022.
17. Price, M. Design Optimization of a Magnesium Subframe. Master's Thesis, Mississippi State University, Starkville, MS, USA, 2018.
18. Liao, J.; Shan, L.; Feng, Y. The Design and Size Optimization of the New FCEV Subframe Based on Hypermesh Platform. *Adv. Mater. Res.* **2011**, *328–330*, 435–440. [[CrossRef](#)]

19. Hamdi, A.; Yannou, B.; Landel, E. Design Target Cascading for Vibro-Acoustic Conceptual Design of An Automobile Subframe. In Proceedings of the DS 32, Proceedings of DESIGN 2004, the 8th International Design Conference, Dubrovnik, Croatia, 17–20 May 2004.
20. Huang, L.; Yuan, C. *Physical Drawbead Design and Modeling with ABAQUS/Isight*; 2017-01-0305; WCX™ 17: SAE World Congress Experience: Detroit, MI, USA, 2017.
21. Coello Coello, C.A. Recent Trends in Evolutionary Multiobjective Optimization. In *Evolutionary Multiobjective Optimization*; Springer: London, UK, 2005; pp. 7–32.
22. Chen, X.; Yu, X.; Ji, B. Study of Crankshaft Strength Based on iSIGHT Platform and DOE Methods. In Proceedings of the 2010 International Conference on Measuring Technology and Mechatronics Automation, Changsha, China, 13–14 March 2010; pp. 548–551.
23. Park, J.S. Optimal Latin-hypercube designs for computer experiments. *J. Stat. Plan. Inference* **1994**, *39*, 95–111. [[CrossRef](#)]
24. Liefvendahl, M.; Stocki, R. A study on algorithms for optimization of Latin hypercubes. *J. Stat. Plan. Inference* **2005**, *136*, 3231–3247. [[CrossRef](#)]
25. Patil, S.A.; Moradi, R.; Lankarani, H.M. Vehicle mass optimization for frontal structure using I-sight and study of weld parameterization for mass improvement. In *ASME International Mechanical Engineering Congress and Exposition*; ASME: New York, NY, USA, 2014; Volume 46613, p. V012T015A011.
26. Fang, H.; Horstemeyer, M.F. Global response approximation with radial basis functions. *Eng. Optim.* **2006**, *38*, 407–424. [[CrossRef](#)]
27. Alsharif, F.; McNaughton, J.L., Jr. Optimization Analysis of a V-Twin Motorcycle Engine Using WAVE Cycle Analysis and an iSight Optimization Framework. In *Ricardo Software e-Brochure V3*; Ricardo, Inc.: Shoreham-by-Sea, UK, 2005; Volume 14, p. 15.
28. Smith, M. *Abaqus User's Manual, Version 2020*; Dassault Systèmes Simulia Corp.: Johnston, RI, USA, 2020.
29. Nicholson, J.C.; Arora, J.S.; Goyal, D.; Tinjum, J.M. Multi-objective structural optimization of wind turbine tower and foundation systems using Isight: A process automation and design exploration software. In Proceedings of the 10th World Congress on Structural and Multidisciplinary Optimization, Orlando, FL, USA, 19–24 May 2013; pp. 19–24.
30. Ren, J.; Zhu, H.W.; Wang, H.; Zhao, C.F.; Zhong, J.L. Multi-objective structural optimization of VL seal ring based on Isight. *J. Phys. Conf. Ser.* **2020**, *1622*, 012031. [[CrossRef](#)]
31. Wang, D.F.; Xie, C.; Liu, Y.C.; Xu, W.C.; Chen, Q. Multi-objective Collaborative Optimization for the Lightweight Design of an Electric Bus Body Frame. *Automot. Innov.* **2020**, *3*, 250–259. [[CrossRef](#)]
32. Richards, Z.D.; Valavanis, K. Particle Swarm trade-off curve analysis for bi-objective optimization. In Proceedings of the IEEE Congress on Evolutionary Computation, Barcelona, Spain, 18–23 July 2010; p. 16.
33. Campbell, F.C. *Fatigue and Fracture: Understanding the Basics*; ASM International: Almere, The Netherlands, 2012.
34. Xu, J.T.; Song, Y.D.; Ding, J.B.; Ding, S.Q. Analysis of a front sub-frame fatigue strength based on Miner theory. In Proceedings of the 2010 International Conference on Computer Application and System Modeling (ICCA SM 2010), Taiyuan, China, 22–24 October 2010.
35. Zhang, L.B.; Liu, Y.; Huang, P.C. FEM-based fatigue analysis method and application in automobile industry. *Comput. Aided Eng.* **2006**, *1*, 195–198.
36. Bignonnet, A.; Thomas, J.J. *Fatigue Assessment and Reliability in Automotive Design*; 2001-01-4061; SAE Brasil International Conference on Fatigue: São Paulo, Brasil, 2001.
37. Peiskammer, D.; Dannbauer, H.; Dutzler, E.; Puchner, K. Using fatigue life prediction to increase reliability of automotive structures. *SAE Trans.* **2003**, *112*, 174–180.
38. Yu, Z.Q.; Jia, H.F.; Huang, X.Y. Design of the Lower Control Arm of an Electric SUV Front Suspension Based on Multi-Disciplinary Optimization Technology. *Jordan J. Mech. Ind. Eng.* **2021**, *15*, 7–14.

**Disclaimer/Publisher's Note:** The statements, opinions and data contained in all publications are solely those of the individual author(s) and contributor(s) and not of MDPI and/or the editor(s). MDPI and/or the editor(s) disclaim responsibility for any injury to people or property resulting from any ideas, methods, instructions or products referred to in the content.